Phase error compensation for a 3-D shape measurement system based on the phase-shifting method

Song Zhang, MEMBER SPIE
Harvard University
Department of Mathematics
Cambridge, Massachusetts 02138
E-mail: szhang77@gmail.com

Peisen S. Huang
State University of New York at Stony Brook
Department of Mechanical Engineering
Stony Brook, New York 11794

Abstract. This paper describes a novel phase error compensation method for reducing the measurement error caused by nonsinusoidal waveforms in phase-shifting methods. For 3-D shape measurement systems using commercial video projectors, the nonsinusoidal waveform of the projected fringe patterns as a result of the nonlinear gamma of projectors causes significant phase measurement error and therefore shape measurement error. The proposed phase error compensation method is based on our finding that the phase error due to the nonsinusoidal waveform depends only on the nonlinearity of the projector's gamma. Therefore, if the projector's gamma is calibrated and the phase error due to the nonlinearity of the gamma is calculated, a lookup table that stores the phase error can be constructed for error compensation. Our experimental results demonstrate that by using the proposed method, the measurement error can be reduced by 10 times. In addition to phase error compensation, a similar method is also proposed to correct the nonsinusoidality of the fringe patterns for the purpose of generating a more accurate flat image of the object for texture mapping. While not relevant to applications in metrology, texture mapping is important for applications in computer vision and computer graphics. [DOI: 10.1117/1.2746814]

Subject terms: 3-D shape measurement; phase shifting; nonsinusoidal waveform; phase error compensation; projector; gamma; lookup table; texture mapping.

Paper 060556R received Jul. 13, 2006; revised manuscript received Nov. 27, 2006; accepted for publication Dec. 6, 2006; published online Jun. 12, 2007. This paper is a revision of a paper presented at the SPIE conference on Two- and Three-Dimensional Methods for Inspection and Metrology III, Oct. 2005, Boston, Mass. The paper presented there appears (unrefereed) in SPIE Proceedings Vol. 6000.

1 Introduction

Various optical methods, such as stereo vision, laser stripe scanning, structured light, and digital fringe projection and phase shifting, have been developed for 3-D shape measurement. Compared to other methods, digital fringe projection and phase-shifting methods have the advantage of high resolution and high measurement speed. They have long been employed in metrology. The measurement accuracy of a 3-D shape measurement system based on fringe image analysis is usually affected by such error sources as the phase-shift error,[1–3] nonsinusoidal waveforms,[4] camera noise and nonlinearity,[5] vibration,[6] and speckle noise.[7]

In digital fringe projection and phase-shifting methods, which use programmable digital video projectors to generate phase-shifted fringe patterns, the phase error due to the phase shift is negligible because of the digital fringe generation. However, the projector's gamma, which represents the relationship between input grayscale values and output grayscale values, is nonlinear. Therefore, if ideal sinusoidal fringe images are sent to the projector, the fringe images produced by the projector are nonsinusoidal. The phase error due to this nonsinusoidal waveform is the single dominant error source. It results from the nonlinearity of the gamma of the projector, and causes significant measurement error. Previously proposed methods, such as the double three-step phase-shifting algorithm[8] and the 3+3 phase-shifting algorithm,[9,10] were able to reduce certain types of phase measurement errors by increasing the number of fringe images. However, the focus of our research is to develop a real-time 3-D shape measurement system.[11] Therefore, increasing the number of fringe images is not desirable. The direct correction of the nonlinearity of the projector's gamma significantly reduced the phase measurement error,[12] but the residual error remains nonnegligible.

We propose a novel phase error compensation method that can produce significantly better results. This method is based on our finding that the phase error due to the nonsinusoidal waveform depends only on the nonlinearity of the projector's gamma. Therefore, if the projector's gamma is calibrated and the phase error due to the nonlinearity of the gamma is calculated, a lookup table (LUT) that stores the phase error can be constructed for error compensation. In addition to phase error compensation, a similar method is also proposed to correct the nonsinusoidality of the fringe

0091-3286/2007/$25.00

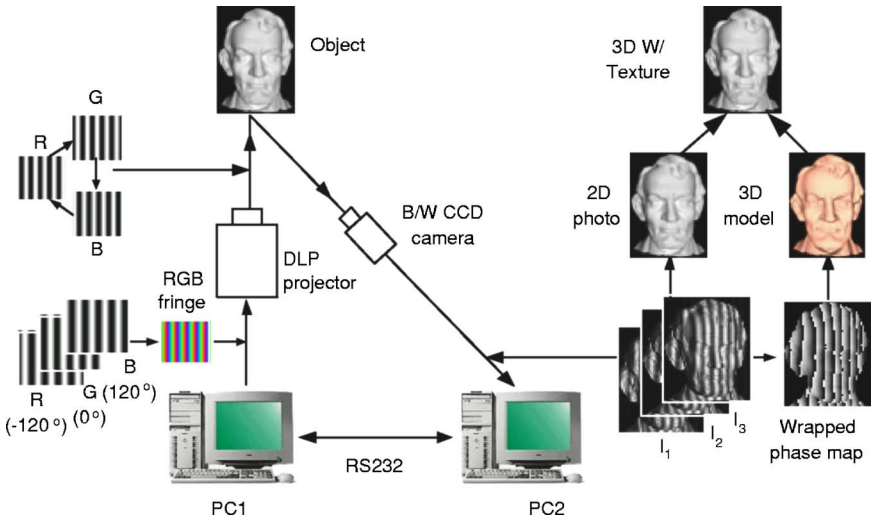

Fig. 1 Schematic diagram of our real-time 3-D shape measurement system.

patterns for the purpose of generating a more accurate flat image of the object for texture mapping, which is important for applications in computer vision and computer graphics.

Section 2 introduces the theoretical background of the proposed method, Secs. 3 and 4 show some simulation and experimental results, and Sec. 5 concludes the paper.

2 Principle

2.1 *Real-Time 3-D Shape Measurement System*

Phase-shifting methods have been used extensively in optical metrology to measure 3-D shapes of objects at various scales. In these methods, a series of phase-shifted sinusoidal fringe patterns are recorded, from which the phase information at every pixel is obtained. This phase information helps determine the correspondence between the image field and the projection field. Once this correspondence is determined, the 3-D coordinates of the object can be retrieved by triangulation.

In our previous research, we developed a high-resolution, real-time 3-D shape measurement system. We simultaneously realized 3-D data acquisition, reconstruction, and display at a speed up to 40 frames/s with a resolution of 532×500.[11] We utilize a single-chip digital light-processing (DLP) projector to generate three-step phase-shifted fringe images. Figure 1 shows the layout of our structured light system for 3-D shape measurement. For a single-chip DLP projector, the color image is produced by projecting the R, G, and B channels sequentially and repeatedly at a high speed. Our eyes then integrate the three color channels into a full color image. To take advantage of this unique projection mechanism of a single-chip DLP projector, we create a color pattern that is a combination of three patterns in the R, G, and B channels, respectively. In the meantime, we remove the color filters on the color wheel of the projector to make the projector operate in a monochrome mode. As a result, when the color pattern is sent to the projector, it is projected as three grayscale patterns, switching rapidly from channel to channel (240 frames/s). A high-speed black-and-white (B/W) camera, which is synchronized with the projector, is used to capture three patterns at 120 frames/s. Based on a three-step phase-shifting algorithm, any three successive fringe images can be used to produce one 3-D shape. The 3-D data acquisition speed is therefore 40 frames/s. Figure 2 shows a picture of the developed hardware system.

2.2 *Three-Step Phase-Shifting Algorithm*

Many different phase-shifting algorithms have been developed.[13] In this research, a three-step phase-shifting algorithm is used, which requires three phase-shifted fringe images. The intensities of three images with a phase shift of $2\pi/3$ are as follows:

$$I_1(x,y) = I'(x,y) + I''(x,y)\cos[\phi(x,y) - 2\pi/3], \tag{1}$$

$$I_2(x,y) = I'(x,y) + I''(x,y)\cos[\phi(x,y)], \tag{2}$$

$$I_3(x,y) = I'(x,y) + I''(x,y)\cos[\phi(x,y) - 2\pi/3], \tag{3}$$

where $I'(x,y)$ is the average intensity, $I''(x,y)$ the intensity modulation, and $\phi(x,y)$ the phase to be determined. Solving Eqs. (1) to (3) simultaneously, we obtain

$$\phi(x,y) = \arctan\left(\sqrt{3}\frac{I_1 - I_3}{2I_2 - I_1 - I_3}\right), \tag{4}$$

$$I'(x,y) = \frac{I_1 + I_2 + I_3}{3}. \tag{5}$$

Here $\phi(x,y)$ is the so-called modulo 2π phase at each pixel, whose value ranges from 0 to 2π. If the fringe patterns contain multiple fringes, phase unwrapping is necessary to remove the sawtooth like discontinuities and obtain a continuous phase map.[14] Once the continuous phase map is obtained, the phase at each pixel can be converted to x, y, z coordinates of the corresponding point through calibration.[15–17] The average intensity $I'(x,y)$ represents a flat image of the object. It can be used for texture mapping in computer vision and graphics applications.

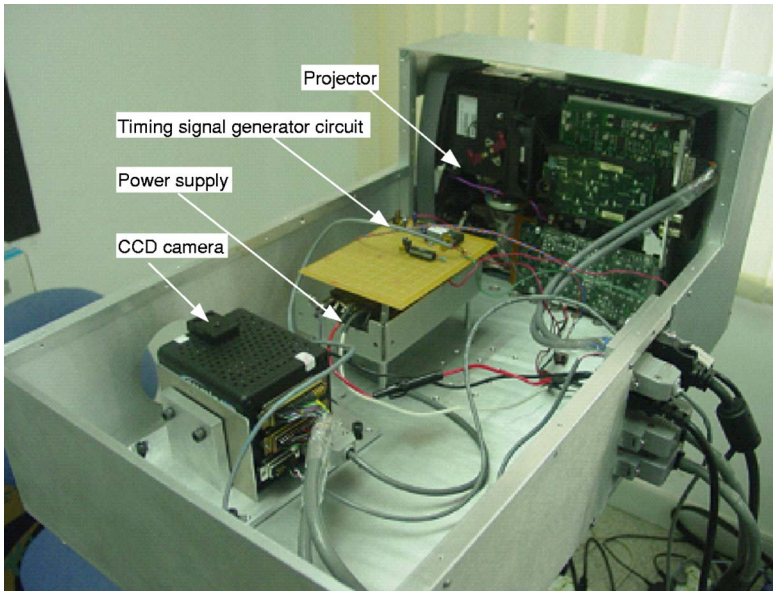

Fig. 2 Photograph of our real-time 3-D shape measurement system.

In this research, a three-step algorithm is implemented in our real-time 3-D shape measurement system.[18] Three phase-shifted fringe patterns are created in R, G, and B channels of a computer-generated color image, but projected as B/W fringe patterns by a digital video projector.

2.3 *Phase Error Compensation*

In this research, the color filters of the projector are removed so that three channels of the projector are projected in 8-bit monochromatic mode. Therefore, the B/W camera reacts to all three channels identically. However, the gamma for each channel of the projector is different. Therefore, the fringe images generated by each channel of the projector have to be considered individually. Images captured by the camera are formed through the procedure illustrated in Fig. 3.

Let us assume that the fringe images generated by the computer with intensities

$$I_k(x,y) = a_0\left\{1+\cos\left[\phi(x,y)+\frac{2(k-2)\pi}{3}\right]\right\}+b_0 \tag{6}$$

are sent to the projector. Here a_0 is the dynamic range of the fringe images, and b_0 the bias. The index $k=1,2,3$ represents the three channels of the projector. The intensities of the fringe images generated by the projector are

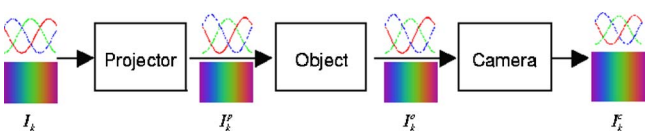

Fig. 3 Fringe image generation procedure.

$$I_k^p(x,y) = f_k(I_k), \tag{7}$$

where $f_k(I_k)$ is a function of I_k that describes the k'th-channel gamma function. If we assume that the projector projects light onto a surface with reflectivity $r_k(x,y)$, and the ambient light that shines on the surface is $a_{1k}(x,y)$, the reflected light intensities are

$$I_k^o(x,y) = r_k(x,y)[I_k^p(x,y)+a_{1k}(x,y)]. \tag{8}$$

In this research, three channels of the projector are projected in grayscale; therefore, the surface reflectivity and the ambient light are the same for all channels. That is, $r_1(x,y)=r_2(x,y)=r_3(x,y)=r(x,y)$ and $a_{11}(x,y)=a_{12}(x,y)=a_{13}(x,y)=a_1(x,y)$. Equation (8) can be rewritten as

$$I_k^o(x,y) = r(x,y)[I_k^p(x,y)+a_1(x,y)]. \tag{9}$$

The reflected light from the object is captured by the B/W camera with a sensitivity of α, which is a constant if the camera is assumed to have a linear response to input light intensities. If the camera response is nonlinear, it can be calibrated independently. The intensities of images captured by the camera are

$$I_k^c(x,y) = \alpha[I_k^o+a_2(x,y)], \tag{10}$$

where $a_2(x,y)$ represents the ambient light that enters the camera directly.

Based on the three-step phase-shifting algorithm, the phase $\phi(x,y)$ can be calculated as follows:

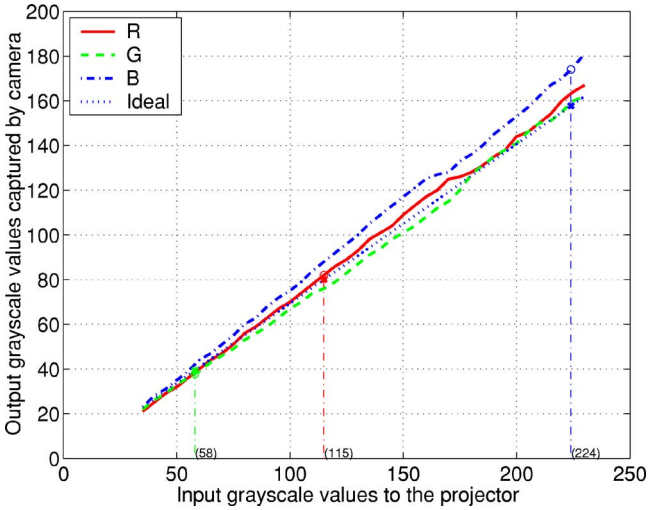

Fig. 4 Calibrated result for the gamma of our projector.

$$\tilde{\phi}(x,y) = \tan^{-1}\left(\sqrt{3}\frac{I_1^c - I_3^c}{2I_2^c - I_1^c - I_3^c}\right)$$
$$= \tan^{-1}\left[\sqrt{3}\frac{f_1(I_1(\phi)) - f_3(I_3(\phi))}{2f_2(I_2(\phi)) - f_1(I_1(\phi)) - f_3(I_3(\phi))}\right]$$
$$= F(\phi). \tag{11}$$

This equation indicates that the phase $\tilde{\phi}(x,y)$ is independent of the response of the camera, the surface reflectivity of objects, and the intensity of ambient light. The phase error due to nonsinusoidal waveforms of the system is only caused by the nonlinearity of the gamma of the projector. If f_1, f_2, and f_3 are monotonic for $\phi \in [0, 2\pi)$, then $F(\phi)$ in Eq. (11) is invertible, that is,

$$\phi(x,y) = F^{-1}(\tilde{\phi}). \tag{12}$$

The phase error caused by the nonlinear gamma is

$$\Delta\phi = \phi - \tilde{\phi} = F^{-1}(\tilde{\phi}) - \tilde{\phi} = g(\tilde{\phi}), \tag{13}$$

where g is a function of $\tilde{\phi}$. Therefore, if the projector's gamma is calibrated and the corresponding phase error is calculated, a LUT that stores the phase error $\Delta\phi$ can be constructed for phase error compensation.

The following steps describe the procedure of constructing such an LUT:

1. Measure the gamma of the projector. A series of grayscale images with different grayscale values $I_n (n = 1, 2, \ldots, N)$ are sent to the projector. The projector projects the grayscale images with intensity values $f_k(I_n)$ onto a whiteboard. The reflected images are captured by the camera, and the intensities at the centers of the captured images, I_{kn}^c, are calculated and recorded. Figure 4 shows a typical example of measured gamma curves for R, G, and B channels of our projector. It is obvious that the curves are nonlinear and unbalanced.
2. Fit the measured points with spline functions $f_k(I)$.
3. Based on the gamma obtained in the previous step, simulate camera-captured images following the procedure illustrated in Fig. 3 under ideal conditions ($a_1 = a_2 = 0$, $\alpha = 1$, and $r = 1$). Calculate the phase $\tilde{\phi}$ using Eq. (11), and the phase error $\Delta\phi$ using Eq. (13).
4. Store the phase and the phase error $(\tilde{\phi}, \Delta\phi)$ in an LUT for phase error compensation.

The phase-error LUT can be used to significantly reduce phase errors in real measurements. Since it depends only on the gamma of the projector, this LUT can be constructed

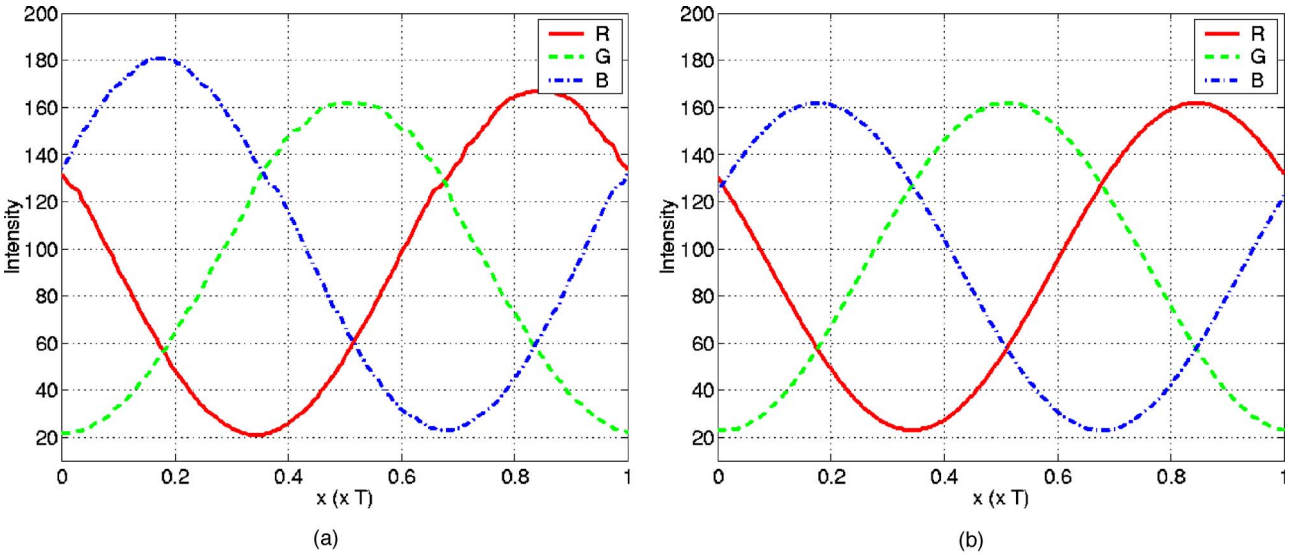

Fig. 5 Cross sections of simulated fringe patterns (a) before and (b) after fringe error correction.

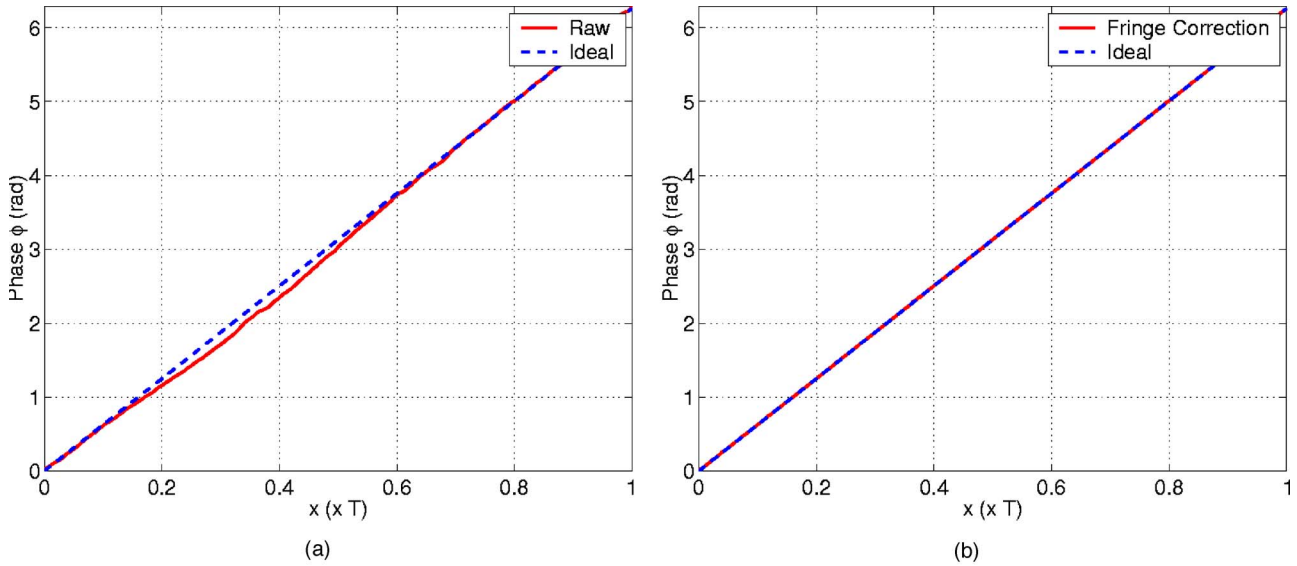

Fig. 6 Phase for the simulated fringe before and after fringe error correction as shown in Fig. 5: (a) computed using the raw simulated fringe shown in Fig. 5(a); (b) computed using the corrected simulated fringe shown in Fig. 5(b).

once for all as long as the gamma is not changed. Moreover, since this phase error compensation method does not require the three functions f_1, f_2, and f_3 to be the same, it can reduce the phase error caused by the imbalance of the three channels. The same method can be applied to correct nonsinusoidal fringe images, which is important for applications that require high-quality texture images, as is discussed in the following subsection.

2.4 *Fringe Error Compensation*

Ideally, the 2-D flat texture image can be generated by simply averaging three phase-shifted fringe images with $2\pi/3$ phase shift. However, if fringe images are not ideally sinusoidal (due to, for example, the nonlinearity of projector gamma), the texture image generated by simple averaging will show residual fringes, which is not desirable for high-quality texture mapping. In this research, we found that the nonsinusoidal fringe images can be corrected by solving a reverse problem.

From discussions in Sec. 2.3, we know that if $f_k(I)$ is monotonic and invertible, $(\tilde{\phi}, f_k(I))$ forms a one-to-one map when $\tilde{\phi} \in [0, 2\pi)$. Therefore, for a given phase value $\tilde{\phi} \in [0, 2\pi)$, its corresponding points $(I_k, f_k(I_k))$ on the

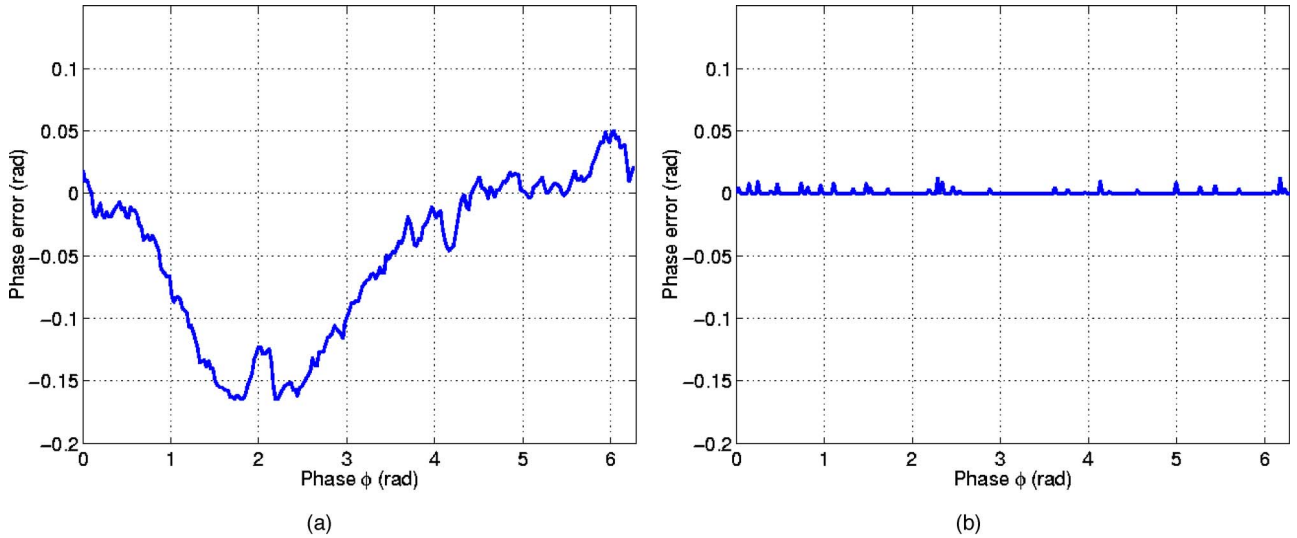

Fig. 7 Phase error before and after phase error correction. (a) Nonsinusoidal phase error before the phase error correction as illustrated in Fig. 6(a). (b) Nonsinusoidal phase error after phase error correction as illustrated in Fig. 6(b).

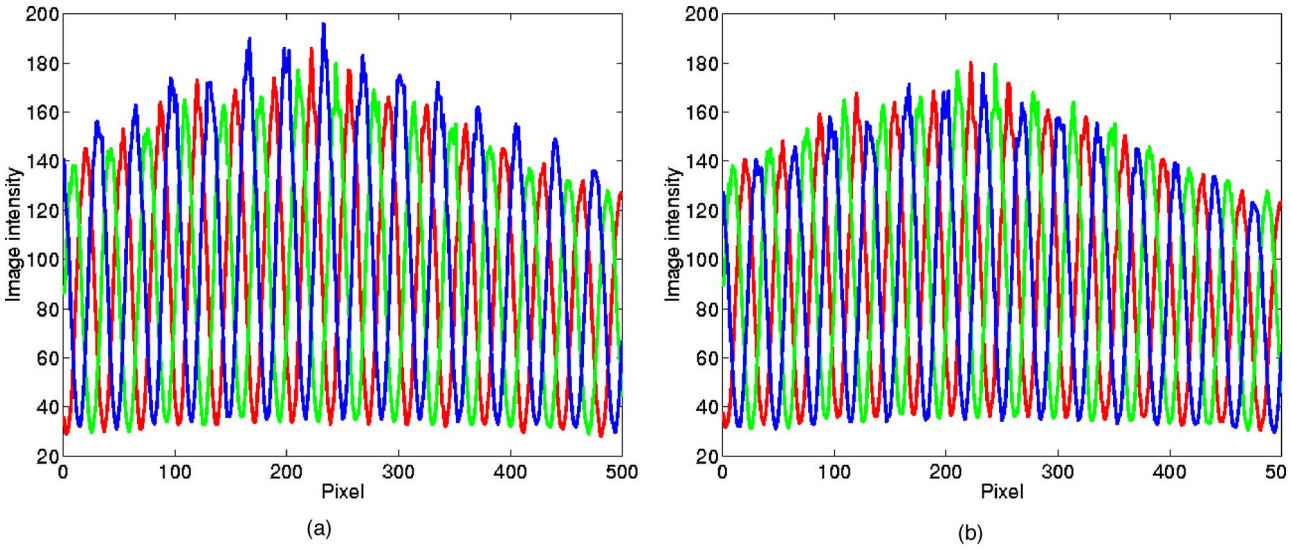

Fig. 8 Fringe correction for real captured fringe images. (a) Cross sections of the fringe images before correction. (b) Cross sections of the fringe images after correction.

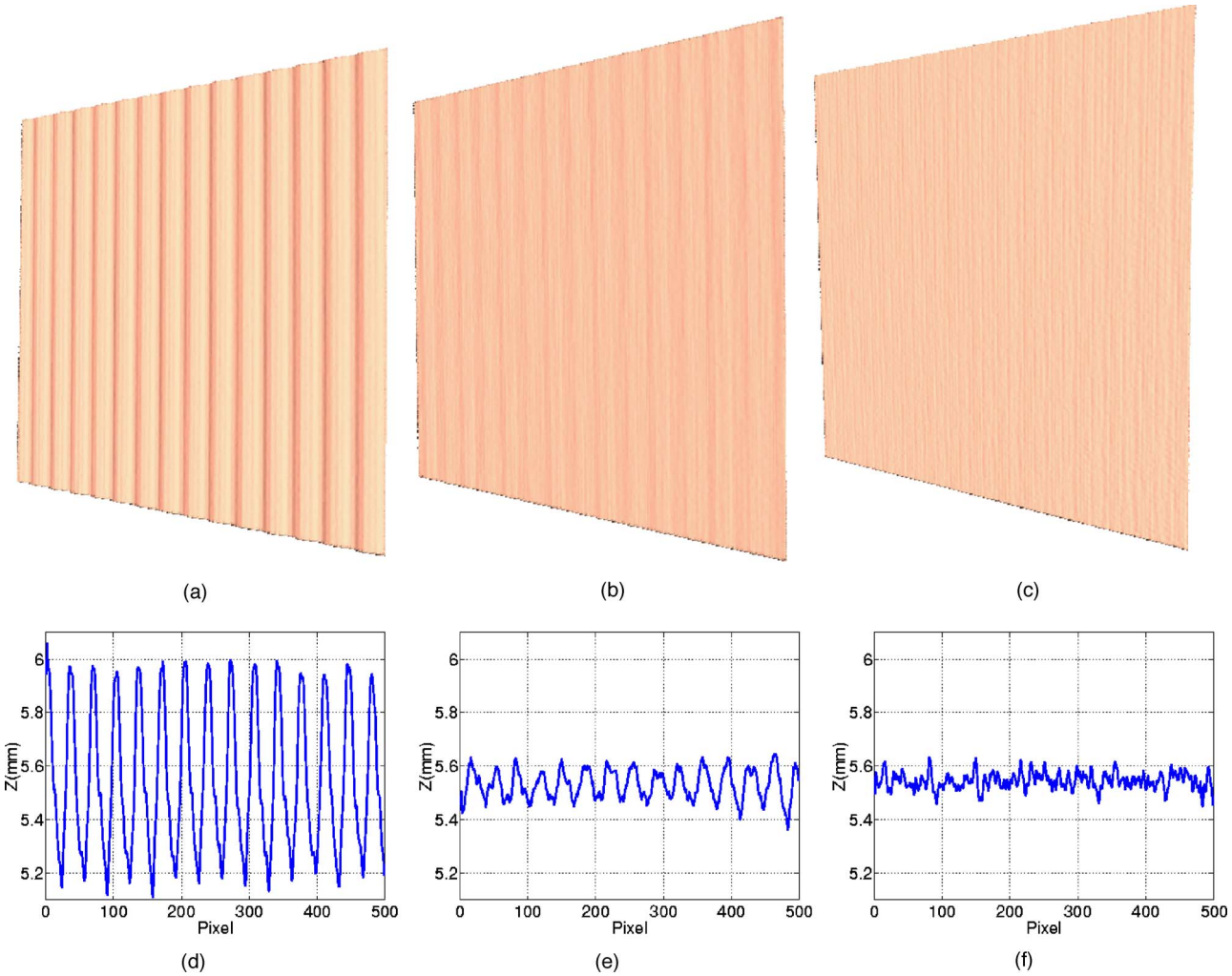

Fig. 9 Reconstructed 3-D geometries of a flat board before and after fringe or phase correction. (a) 3-D geometry before correction. (b) 3-D geometry after fringe error correction only, as explained in Sec. 2.4. (c) 3-D geometry after phase error correction only, as explained in Sec. 2.3. (d)–(f) Cross sections of the corresponding 3-D geometries in (a)–(c).

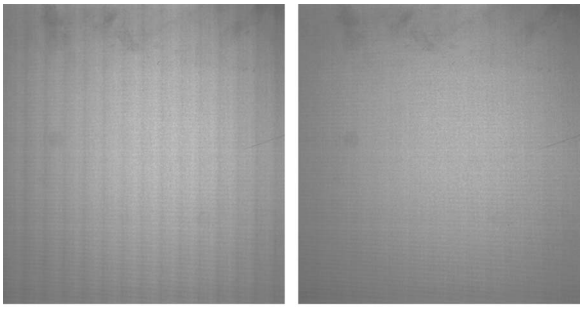

Fig. 10 2-D texture images (a) before and (b) after fringe error correction. The averaged 2-D image has stripes before correcting the fringes; the stripes are significantly reduced after fringe error correction.

gamma can be uniquely determined. Now let us define an ideal gamma $\hat{f}(I)$, which is a straight line, for all channels with the starting and ending points defined as follows:

$$\hat{f}(I_1) = \max\{f_k(I_1)\}, \tag{14}$$

$$\hat{f}(I_N) = \min\{f_k(I_N)\}. \tag{15}$$

Then the corresponding points of the same $\tilde{\phi}$ on the ideal gamma curves $(I_k \hat{f}(I_k))$ can also uniquely determined. This means that the ratio

$$R_k = \frac{f_k(I_k)}{\hat{f}(I_k)}, \tag{16}$$

which we call the gamma ratio, is uniquely defined for any given $\tilde{\phi}$. Therefore, we can build a gamma-ratio LUT $(\tilde{\phi}, R_k)$ to correct the nonsinusoidal fringe images, and to produce the texture image by averaging the corrected fringe images.

The following steps describe the procedure of constructing such an LUT:

1. Follow steps 1 to 3 in the procedure of constructing the phase-error LUT to find the phase value $\tilde{\phi}$.
2. Find the ideal gamma function $\hat{f}(I)$ based on the definition in Eqs. (14) and (15).
3. Find the corresponding points of each phase value $\tilde{\phi} \in [0, 2\pi)$ on three gamma functions $(I_k, f_k(I_k))$ and the ideal gamma functions $(I_k, \hat{f}(I_k))$.
4. Calculate the gamma ratio R_k, and store $(\tilde{\phi}, R_k)$ in an LUT for fringe image correction.

To explain how this gamma-ratio LUT can be used to correct nonsinusoidal fringe images and make them sinusoidal, we use an example for the case when the phase value is $\pi/4$. The corresponding points of this phase value on the measured R, G, and B gamma curves are (115, 82.00), (58, 37.80), and (224, 174.00), respectively, as shown in Fig. 4. The ideal gamma function is

$$\hat{f}(I) = \frac{162 - 23}{230 - 35}(I - 35) + 23. \tag{17}$$

Using this equation, we can calculate the grayscale values of corresponding points on the ideal gamma function; they are (115, 80.03), (58, 39.39), and (224,157.72), respectively. The gamma ratios are then calculated according to Eq. (16) as

$$\{(0.9760, 1.0421, 0.9064) | \tilde{\phi} = \pi/4\}.$$

These gamma-ratio values are stored in the gamma-ratio LUT and used in a real measurement to correct the grayscale values of the fringe images at any pixel whose phase value is $\tilde{\phi} = \pi/4$. After the fringe images are corrected to be ideally sinusoidal, we can then average them to generate the flat image of the object for high-quality texture mapping.

3 Simulation Results

Figure 4 shows a typical gamma for our projector. The usable grayscale values range from 35 to 235. Beyond this range, the curves are almost flat and cannot be used. As a simulation, we use this gamma to generate three phase-shifted fringe patterns with a phase shift of $2\pi/3$ in the projector's R, G, and B channels, respectively. The input fringe patterns are as follows:

$$I_k(x,y) = 100\left\{1 + \cos\left[\frac{2\pi x}{p} + \frac{2(k-2)\pi}{3}\right]\right\} + 35, \tag{18}$$

where $k = 1, 2, 3$ represents the three color channels, and p is the fringe pitch. After projection, the fringe patterns are transformed by gamma functions. Figure 5(a) shows cross sections of the simulated fringe patterns. After the fringe correction algorithm is applied, cross sections of the same fringe patterns are shown in Fig. 5(b). It is clear that after correction, the three fringe patterns become more sinusoidal in shape and also better balanced in intensity. The phase is computed from these fringe patterns as shown in Fig. 6. Figure 6(a) shows the result before error correction, while Fig. 6(b) shows the result after correction. It can be seen clearly that the phase is closer to the ideal phase after the error correction.

If we use the simulated fringe patterns before correction to compute the phase map directly, the phase error is approximately 0.27 rad peak-to-peak, as shown in Fig. 7(a). After phase error compensation using the constructed phase-error LUT, the phase error is reduced to 0.01 rad as shown in Fig. 7(b). Correcting the fringe or the phase does not make any difference in simulation. However, for real captured images, the corrected and uncorrected results are slightly different due to the existence of the ambient light, $a_1(x,y)$ and $a_2(x,y)$, as is explained in the next section.

4 Experiments

Our simulation results show that we can use LUTs to reduce phase error and correct fringe images. To verify that this method works in real systems, we implemented the algorithms in our real-time 3-D shape measurement system.[18] We first measured a flat board. The result is shown in Fig. 8. Figure 8(a) shows cross sections of ac-

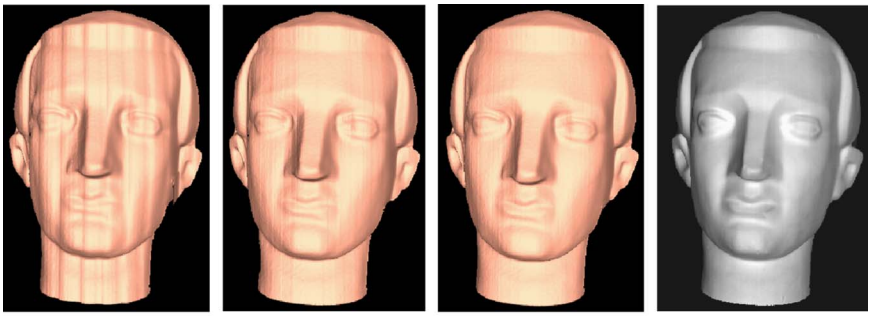

Fig. 11 Reconstructed 3-D geometries of the head model before and after fringe or phase correction: (a) before correction, (b) after fringe correction, (c) after phase correction, (d) with corrected texture mapping.

quired fringe images. The fringe patterns were projected by a projector with the gamma shown in Fig. 4. We see that the three fringe images are not well balanced. Figure 8(b) shows the cross sections of fringe images after correction, which are better balanced.

Figure 9 shows a comparison of the reconstructed 3-D results before and after fringe or phase correction. Before correction, the root-mean-square (rms) measurement error is approximately 0.25 mm, as shown in Fig. 9(a). Figure 9(b) shows the measurement result after correcting fringe images directly using the method introduced in Sec. 2.4. Figure. 9(c) shows the measurement results after phase error correction; the measurement error is approximately 0.025 mm rms, which is 10 times smaller than that before correction. It is clear that correcting the phase error directly results in higher accuracy than correcting fringe images. We believe that this difference is due to the existence of ambient light, $a_1(x,y)$ and $a_2(x,y)$.

The texture images before and after fringe correction are shown in Fig. 10. The texture image before correction shows vertical stripes. After correction, the stripes are barely seen and the image quality is sufficient for texture mapping.

We also measured a plaster head model. Figure 11 shows the reconstructed 3-D geometry before and after correction. The reconstructed 3-D geometric surface after phase correction or phase error compensation is very smooth. Figure 11(a) shows the reconstructed 3-D geometry before correction. Figure 11(b) shows the 3-D geometry reconstructed by using the compensated fringe images. Figure 11(c) shows the 3-D geometry after correcting phase error directly. Figure 11(d) is the 3-D result with corrected texture mapping. These experimental results confirmed that the error correction algorithms improved the accuracy of measurement and reduced stripe patterns in the texture image.

It should be noted that the phase error correction algorithm introduced in this work is independent of the measurement depth z or the orientation of the board, since all the corrections are performed in phase domain to compensate the gamma effect of the projector. However, if the projector is significantly blurred, the fringe correction might be affected, since the nonsinusoidal fringe will be sinusoidal once the fringe patterns are sufficiently blurred (no fringe correction is actually necessary for this case).

5 Conclusions

This paper has introduced a novel phase error compensation method for a 3-D shape measurement system based on a phase-shifting method. In this system, the phase-shifted fringe patterns are generated by a video projector. The main error source of this system is the nonlinearity of the projector's gamma, which results in nonsinusoidal waveforms in the fringe patterns and causes phase error in measurements. Our analysis showed that the phase error in the measurement is caused only by the nonlinearity of the projector's gamma. Therefore, to eliminate phase error, we proposed a compensation method that uses an LUT to store the phase error calculated from the calibrated gamma of the projector. Our experimental results demonstrated that by using the proposed method, the measurement error could be reduced by 10 times. Moreover, the method can not only reduce the phase error due to nonsinusoidal waveform, but also reduce the phase error caused by the imbalance of fringe images. In fact, we can verify that this method can reduce any type of error caused by the projector's gamma.

In addition to phase error compensation, a similar LUT method was also proposed to correct the nonsinusoidality of fringe patterns for the purpose of generating a more accurate flat image of the object for texture mapping.

Acknowledgments

This work was supported by the National Science Foundation under grant No. CMS-9900337 and the National Institute of Health under grant No. RR13995.

When this work was done, Song Zhang was with the Department of Mechanical Engineering, State University of New York at Stony Brook.

References

1. J. Schwider, T. Dresel, and B. Manzke, "Some considerations of reduction of reference phase error in phase-stepping interferometry," *Appl. Opt.* **38**, 655–658 (1999).
2. C. Joenathan, "Phase-measuring interferometry: new methods and error analysis," *Appl. Opt.* **33**, 4147–4155 (1994).
3. P. Hariharan, "Phase-shifting interferometry: minimization of system errors," *Appl. Opt.* **39**, 967–969 (200l).

4. K. Hibino, B. F. Oreb, D. I. Farrant, and K. G. Larkin, "Phase shifting for nonsinusoidal waveforms with phase-shift errors," *J. Opt. Soc. Am. A* **12**, 761–768 (1995).
5. T. Maack and R. Kowarschik, "Camera influence on the phase-measuring accuracy of a phase-shifting speckle interferometry," *Appl. Opt.* **35**, 3514–3524 (1996).
6. P. L. Wizinowich, "Phase-shifting interferometry in the presence of vibration: a new algorithm and system," *Appl. Opt.* **29**, 3271–3279 (1990).
7. B. Trolard, "Speckle noise removal in interference fringes by opto-electronic preprocessing with Epson liquid crystal television," in *Proc. SPIE* **2860**, 126–134 (1996).
8. P. S. Huang, Q. Hu, and F.-P. Chiang, "Double three-step phase-shifting algorithm," *Appl. Opt.* **41**, 4503–4509 (2002).
9. J. Schwider, R. Burow, J. Elssner, K. E. abd Grzanna, R. Spolaczyk, and K. Merkel, "Digital wave-front measuring interferometry: some systematic error sources," *Appl. Opt.* **22**, 3421–3432 (1983).
10. J. C. Wyant and K. N. Prettyjohns, "Optical profiler using improved phase-shifting interferometry," U.S. Patent 4,639,139 (1987).
11. S. Zhang, "High-resolution, real-time 3-D shape measurement," PhD Thesis, Stony Brook Univ., Stony Brook, NY (2005).
12. P. S. Huang, C. Zhang, and F. P. Chiang, "High-speed 3-D shape measurement based on digital fringe projection," *Opt. Eng.* **42**, 163–168 (2003).
13. D. Malacara, Ed., *Optical Shop Testing*, John Wiley and Sons, New York (1992).
14. D. C. Ghiglia and M. D. Pritt, *Two-Dimensional Phase Unwrapping: Theory, Algorithms, and Software*, John Wiley and Sons, Inc. (1998).
15. S. Zhang and P. S. Huang, "Novel method for structured light system calibration," *Opt. Eng.* **45**, 083601-1-8 (2006).
16. R. Legarda-Sáenz, T. Bothe, and W. P. Jüptner, "Accurate procedure for the calibration of a structured light system," *Opt. Eng.* **43**, 464–471 (2004).
17. Q. Hu, P. S. Huang, Q. Fu, and F. P. Chiang, "Calibration of a 3-D shape measurement system," *Opt. Eng.* **42**, 487–493 (2003).
18. S. Zhang and P. Huang, "High-resolution, real-time 3-D shape acquisition," in *IEEE Computer Vision and Pattern Recognition Workshop on Realtime 3D Sensors and Their Uses*, Vol. **3**, pp. 28–37 (2004).

Song Zhang is a postdoctoral fellow at Harvard University. He received his PhD degree in mechanical engineering from Stony Brook University in 2005. He has authored or coauthored more than 30 research articles in journals, conference proceedings, workshops, and exhibitions. He serves as referee for *Optics Letters and for Optics and Laser Technology*. His research interests include real-time optical metrology, 3-D machine and computer vision, computer graphics, human-computer interaction, virtual reality, and differential geometry.

Peisen S. Huang obtained his BS degree in precision instrumentation engineering from Shanghai Jiao Tong University, China, in 1984; his ME and Dr Eng degrees in precision engineering and mechatronics from Tohoku University, Japan, in 1988 and 1995, respectively; and his PhD degree in mechanical engineering from the University of Michigan, Ann Arbor, in 1993. He has been a faculty member in the Department of Mechanical Engineering, Stony Brook University, since 1993. His research interests include optical metrology, image processing, and 3-D computer vision.